

Supporting Information

Gradient engineered hole-transporting material for monolithic series-type large-area perovskite solar cells

Yongguang Tu ^a, Jihuai Wu ^{a*}, Xin He ^a, Panfeng Guo ^a, Tongyue Wu ^a, Hui Luo ^a, Quanzhen Liu ^a, Qihui Wu ^b,

Jianming Lin ^a, Miaoliang Huang ^a, Zhang Lan ^a, Sizhong Li ^a

^aEngineering Research Center of Environment-Friendly Functional Materials for Ministry of Education, Key

Laboratory of Functional Materials for Fujian Higher Education, College of Material Science and Engineering,

Huaqiao University, Xiamen 361021, Fujian, People's Republic of China

^bDepartment of Materials Chemistry, College of Chemical Engineering and Materials Science, Quanzhou Normal

University, Quanzhou 362000, Fujian, People's Republic of China

Figure S1-S4

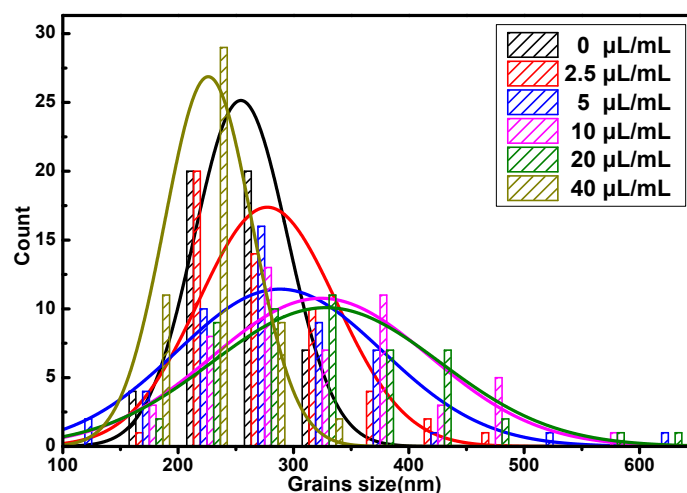


Figure S1 Histogram of perovskite grain size for anti-solution concentration from 0 $\mu\text{L/mL}$ to 40 $\mu\text{L/mL}$.

*Corresponding author. Tel: +86-595-22693899; Fax: +86-595-22692229; E-mail address: jhwu@hqu.edu.cn (J. Wu).

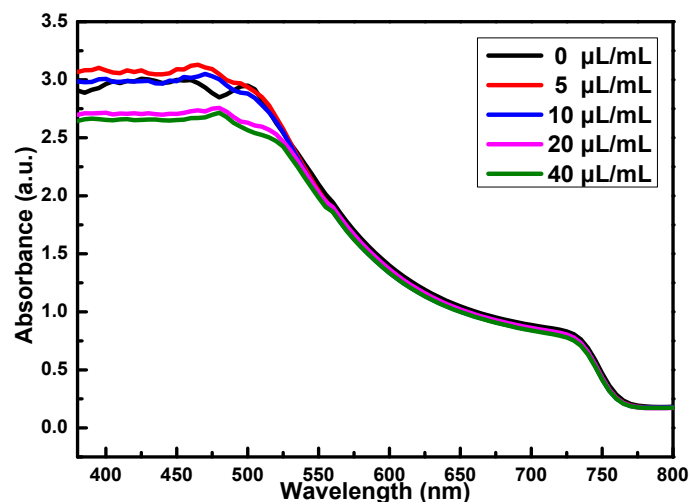
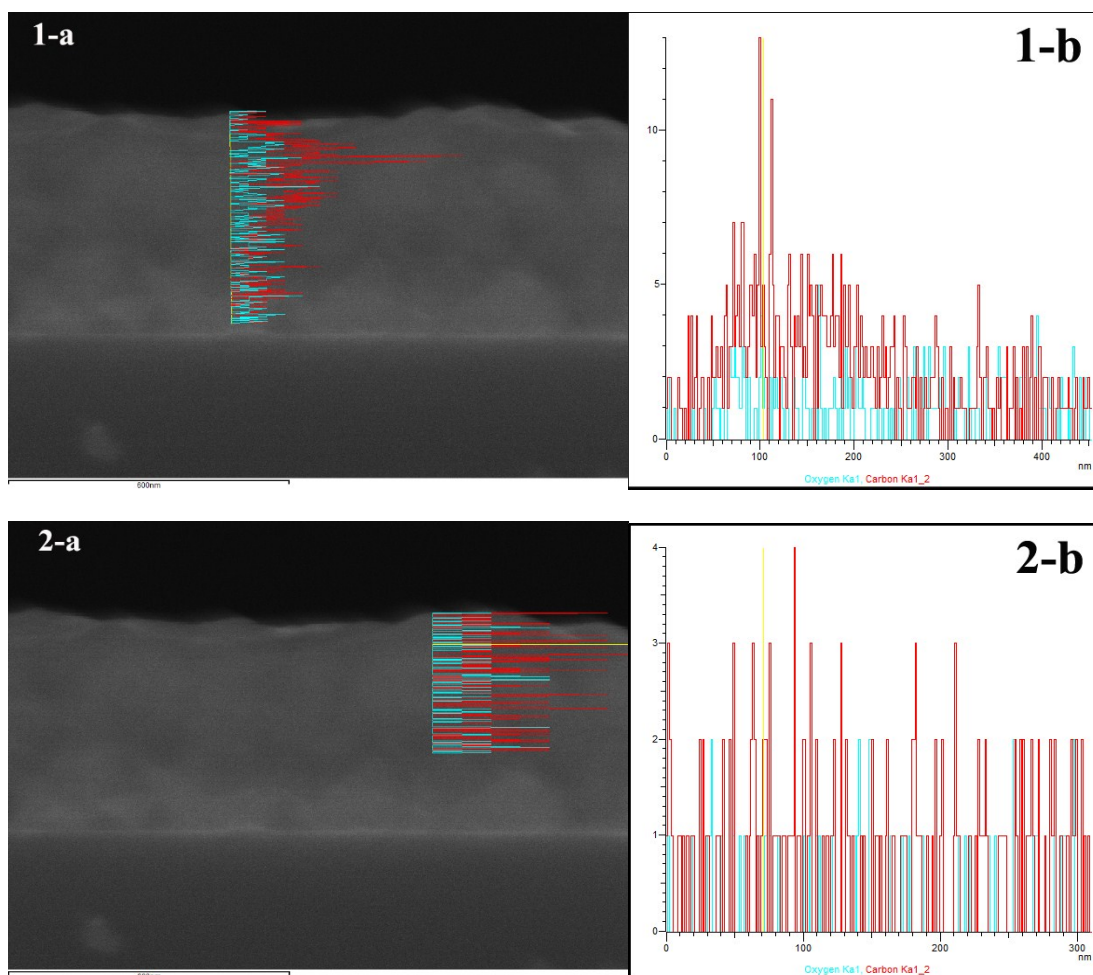


Figure S2 UV-vis absorption spectras of perovskite films.



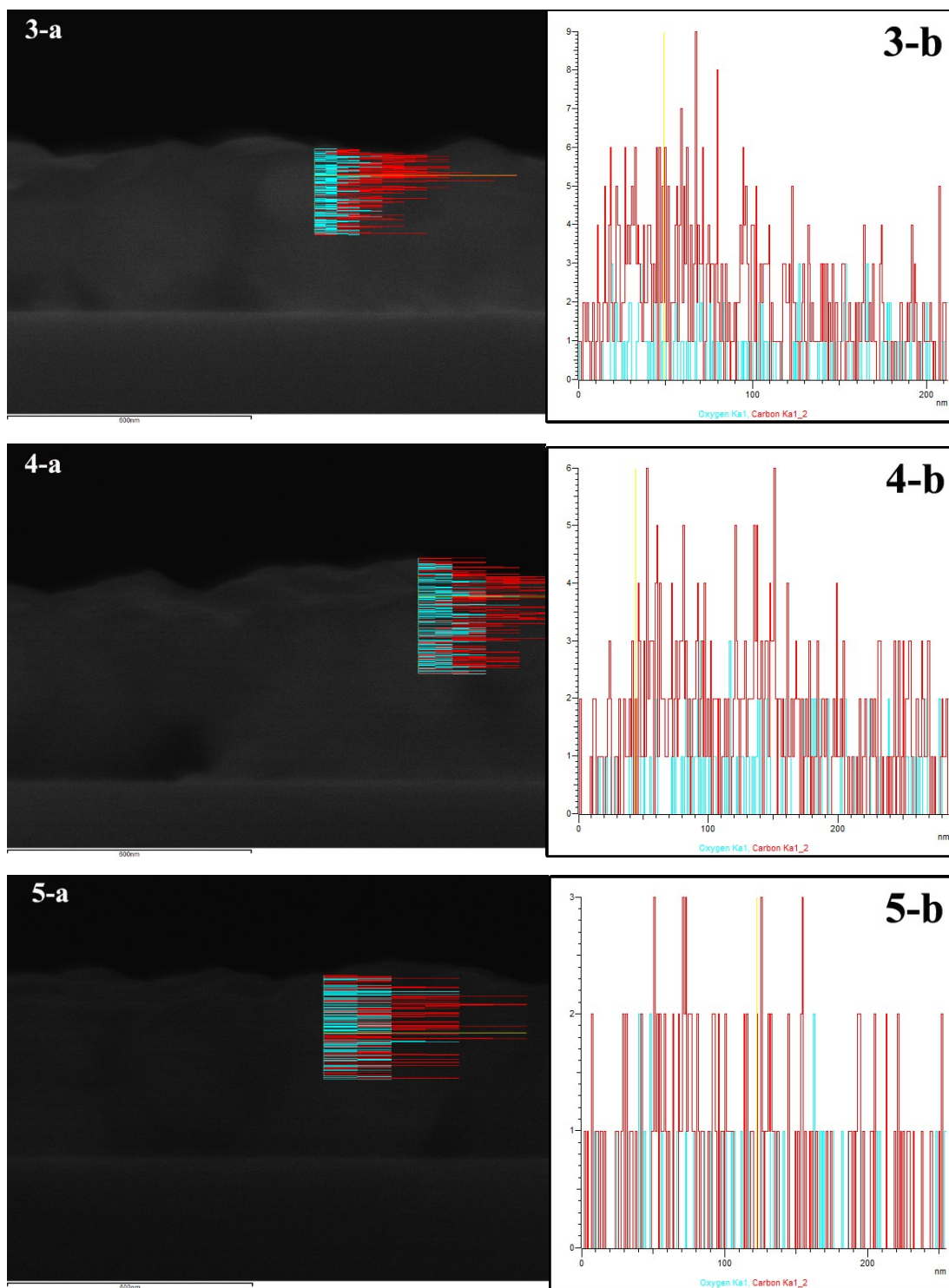


Figure S3 Energy-dispersive X-ray spectroscopy (EDX) mapping of perovskite film based on 10 $\mu\text{L/mL}$.

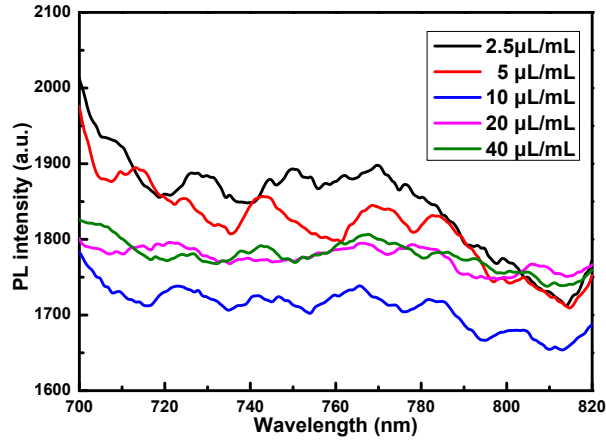


Figure S4 Magnification steady state photoluminescence spectra of perovskite films on non-conducting glass detected at 460 nm excitation wavelength.

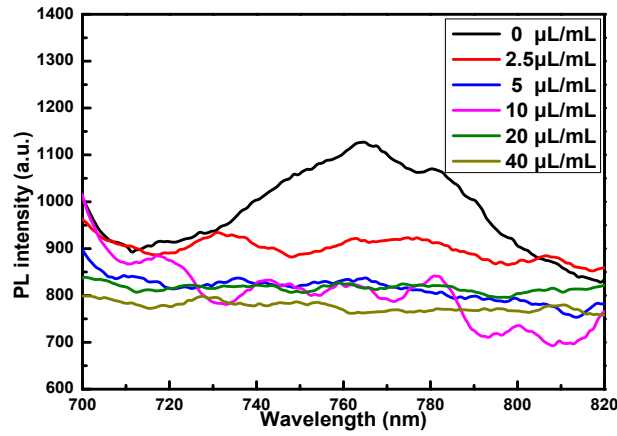


Figure S5 Steady state photoluminescence spectra based on perovskite/PEDOT:PSS/ non-conducting glass detected at 460 nm excitation wavelength.

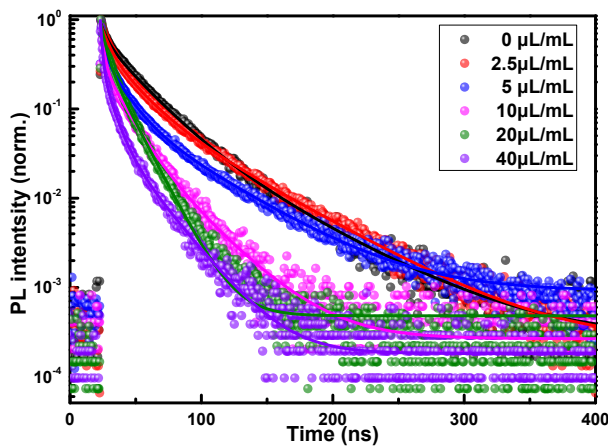


Figure S6 Time-resolved photoluminescence intensity decay spectra based on perovskite/PEDOT:PSS/ non-conducting glass detected at 760 nm emission wavelength.

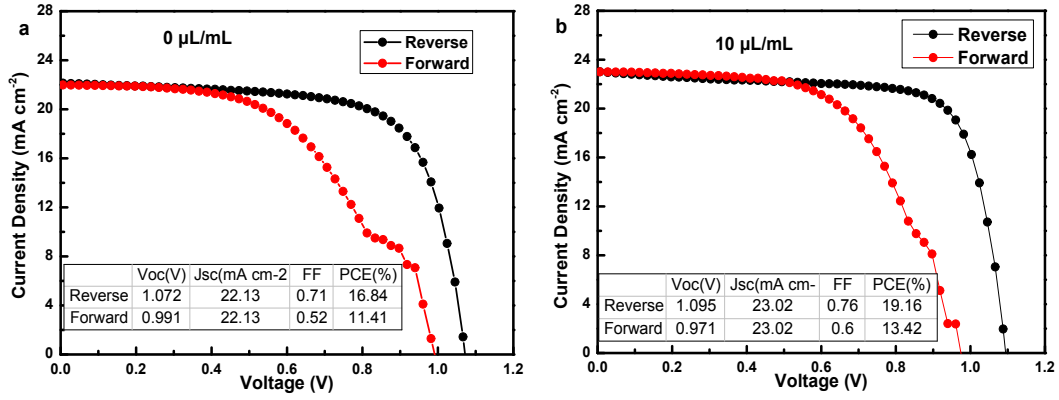


Figure S7 J-V curves of the devices based on 0 $\mu\text{L/mL}$ and 10 $\mu\text{L/mL}$ measured by reverse (open circuit \rightarrow short circuit) and forward (short circuit \rightarrow open circuit) scans under AM 1.5 G illumination. (a) 0 $\mu\text{L/mL}$, (b) 10 $\mu\text{L/mL}$.

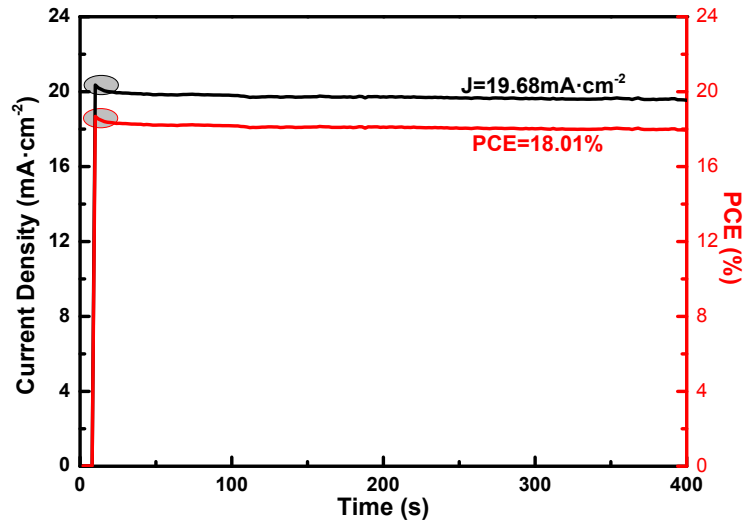
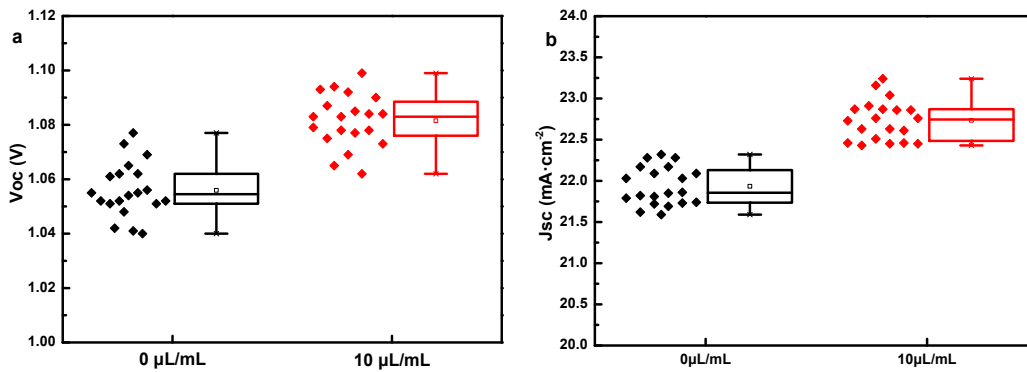


Figure S8 The steady-state photocurrent and output PCE of the champion devices at the maximum power points.



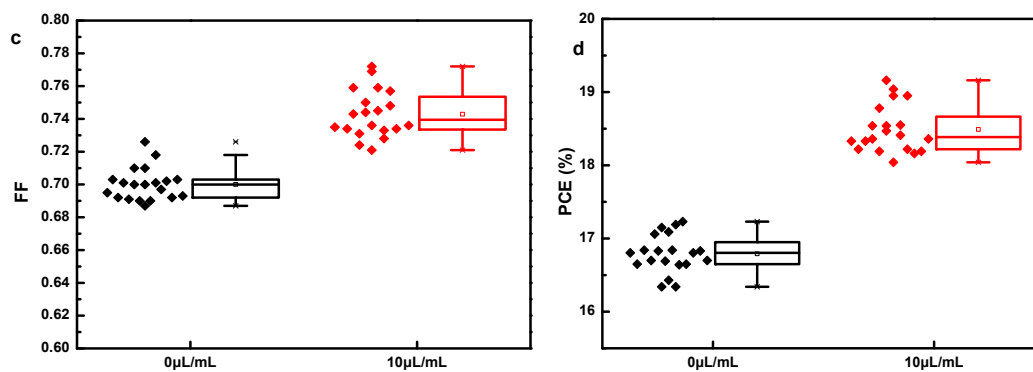


Figure S9 Boxes charts of photovoltaic parameters. (a) Voc, (b) Jsc, (c) FF and (d) PCE extracted from J-V measurements of the solar cells based on 0 μL/mL and 10 μL/mL (Each parameters is calculated from a batch of 25 cells).

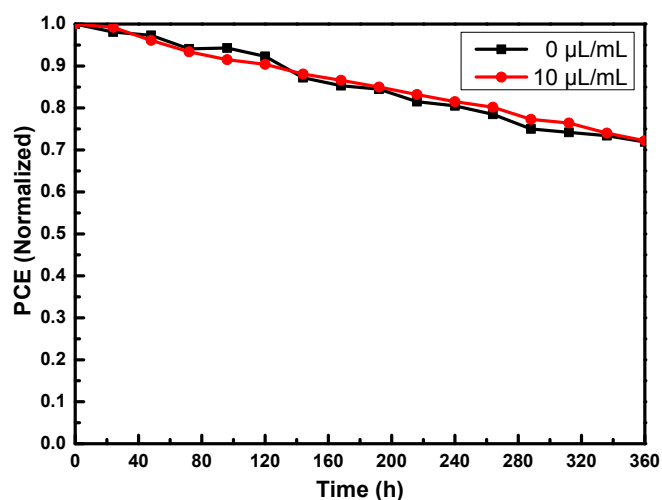


Figure S10 Stability of the devices based on 0 μL/mL and 10 μL/mL in an ambient environment without encapsulation.

Table S1 The Spiro-OMeTAD content in the anti-solution.

Spiro-OMeTAD Concentration (μL/mL)	0	2.5	5	10	20	40
Spiro-OMeTAD Content (mg/mL)	0	0.18	0.36	0.72	1.44	2.88

Table S2 Fitting parameters for the time-resolved PL measurements by using two exponential model shown in Figure 7.

Sample	A ₁	τ ₁ /ns	A ₂	τ ₂ /ns	Average τ/ns
0 μL/mL	55.69%	6.130	44.31%	54.572	27.597
2.5 μL/mL	62.83%	7.551	37.17%	48.986	22.952
5 μL/mL	55.77%	6.108	44.23%	42.978	22.416
10 μL/mL	57.98%	4.693	42.02%	33.713	16.887
20 μL/mL	64.99%	2.965	35.01%	28.683	11.969
40 μL/mL	65.51%	3.402	34.49%	26.505	11.370

Table S3 Fitting parameters for the time-resolved PL measurements by using two exponential model shown in Figure S6.

Sample	A ₁	τ ₁ /ns	A ₂	τ ₂ /ns	Average τ/ns
0 μL/mL	52.05%	4.307	47.95%	29.151	16.220
2.5 μL/mL	48.62%	4.508	51.38%	27.246	16.190
5 μL/mL	56.31%	2.800	43.69%	24.039	12.079
10 μL/mL	60.24%	1.922	39.76%	16.977	7.908
20 μL/mL	72.46%	3.175	27.54%	13.914	6.133
40 μL/mL	66.21%	1.257	33.79%	10.940	4.529

The PL decay can be fitted by a two-component exponential decay function:

$$y = y_0 + A_1 \exp(-t/\tau_1) + A_2 \exp(-t/\tau_2)$$

where τ₁ (τ₂) represents the decay time of fast (slow) decay; A₁ (A₂) represents the amplitude of the fast -decay (slow -decay) component.